

*Annual Review of Analytical Chemistry*  
**Probing and Visualizing  
Interfacial Charge at Surfaces  
in Aqueous Solution**

Giada Caniglia,<sup>1,\*</sup> Gözde Tezcan,<sup>2,\*</sup> Gabriel N. Meloni,<sup>2</sup>  
Patrick R. Unwin,<sup>2</sup> and Christine Kranz<sup>1</sup>

<sup>1</sup>Institute of Analytical and Bioanalytical Chemistry, Ulm University, Ulm, Germany;  
email: christine.kranz@uni-ulm.de

<sup>2</sup>Department of Chemistry, University of Warwick, Coventry, United Kingdom;  
email: p.r.unwin@warwick.ac.uk

Annu. Rev. Anal. Chem. 2022. 15:247–67

First published as a Review in Advance on  
March 8, 2022

The *Annual Review of Analytical Chemistry* is online at  
anchem.annualreviews.org

<https://doi.org/10.1146/annurev-anchem-121521-122615>

Copyright © 2022 by Annual Reviews.  
All rights reserved

\*These authors contributed equally to this article

ANNUAL  
REVIEWS **CONNECT**

[www.annualreviews.org](http://www.annualreviews.org)

- Download figures
- Navigate cited references
- Keyword search
- Explore related articles
- Share via email or social media

### Keywords

surface charge density, atomic force microscopy, scanning ion conductance microscopy, electrical double layer, electrified interfaces

### Abstract

Surface charge density and distribution play an important role in almost all interfacial processes, influencing, for example, adsorption, colloidal stability, functional material activity, electrochemical processes, corrosion, nanoparticle toxicity, and cellular processes such as signaling, absorption, and adhesion. Understanding the heterogeneity in, and distribution of, surface and interfacial charge is key to elucidating the mechanisms underlying reactivity, the stability of materials, and biophysical processes. Atomic force microscopy (AFM) and scanning ion conductance microscopy (SICM) are highly suitable for probing the material/electrolyte interface at the nanoscale through recent advances in probe design, significant instrumental (hardware and software) developments, and the evolution of multifunctional imaging protocols. Here, we assess the capability of AFM and SICM for surface charge mapping, covering the basic underpinning principles alongside experimental considerations. We illustrate and compare the use of AFM and SICM for visualizing surface and interfacial charge with examples from materials science, geochemistry, and the life sciences.

Downloaded from [www.annualreviews.org](http://www.annualreviews.org).

Guest (guest)

IP: 3.133.12.172

247

On: Sun, 05 May 2024 04:37:44

## INTRODUCTION

Understanding the properties of solid-liquid interfaces at materials immersed in electrolyte solution is essential for applications spanning mineral processing, corrosion sciences, electrochemistry, (photo)catalysis, and the life sciences. Electrostatic interactions between particles, originating from surface charge, have a direct effect on aggregation, flocculation, and coagulation (1), and colloidal stability is significantly influenced by the electrostatic repulsion of particles. The adhesion of cells and the adsorption of biomolecules, such as proteins and nucleic acids, at surfaces are strongly dependent on the surface charge (2).

Regardless of the nature of the sample, electrified solid-liquid interfaces are usually described as an arrangement of ions and solvent molecules forming an electrical double layer (EDL) adjacent to a charged surface. The surface charge can arise, e.g., by dissociation (ionization) of chemical groups at the surface or by specific adsorption of ions from the surrounding solution (3). In electrochemical systems, metal or semiconductor electrodes bear charges with respect to the solution, depending on the electrode potential (4). While surface charge and surface potential measurements have a long history, especially in colloid science (5) and electrochemistry (6), measurements are typically on bulk populations of particles or extended surfaces via titration (7), impedance (8), electrokinetic (9), and surface force apparatus measurements (10).

Charge heterogeneities, e.g., between particles or within a single particle, are much more challenging to measure. Optical methods, e.g., using fluorescent nanoparticles as labels (11, 12), have been used to detect variations of surface charge at the surfaces of cells and membranes, and photoelectrochemical imaging to map surface charge at the cell-support surface has also recently been proposed (13). These are suitable approaches for biological samples but require labeling or particular supports.

There is a significant body of literature reporting scanning probe microscopy (SPM) techniques mainly operated in high vacuum or air (ambient conditions) to determine local surface potential and charge with nanoscale resolution (14–17). In contrast, scanning ion conductance microscopy (SICM) and atomic force microscopy (AFM) have seen tremendous progress for locally studying solid-liquid interfaces and surface charge density (18–31).

In this review, we present SICM and AFM for mapping surface charge at various samples in aqueous electrolyte solution, focusing on principles of operation, giving a brief overview on the theoretical background, and describing recent applications. In addition, we contrast the main differences and complementarity of the two techniques with respect to surface charge mapping and highlight future promising developments for both techniques.

## THE ELECTRICAL DOUBLE LAYER

The EDL is usually described by classical mean-field models like the Gouy–Chapman–Stern (GCS) model (3), which combines the Helmholtz model [a parallel-plate capacitor, neglecting specifically adsorbed species, defining the Stern layer or inner Helmholtz ( $H_i$ ) and outer Helmholtz ( $H_o$ ) layer] and the Gouy–Chapman (GC) model (diffuse layer), which is given by the Debye length ( $\lambda_D$ ):

$$\lambda_D = \sqrt{\left( \varepsilon_0 \varepsilon_r k_B T / \sum_{j=1}^N c_j^0 q_j^2 \right)}, \quad 1.$$

where  $\varepsilon_r$  and  $\varepsilon_0$  are the relative dielectric constant of the medium and the vacuum permittivity, respectively,  $k_B$  is the Boltzmann constant,  $T$  is the absolute temperature,  $c_j^0$  and  $q_j$  are the bulk concentration and the charge of species  $j$ , and  $N$  is total number of charged species. With an increasing concentration ( $c_j^0$ ),  $\lambda_D$  decreases due to effective screening of the surface charge by the ions in solution.

Downloaded from www.annualreviews.org.

Guest (guest)

IP: 3.133.12.172

On: Sun, 05 May 2024 04:37:44

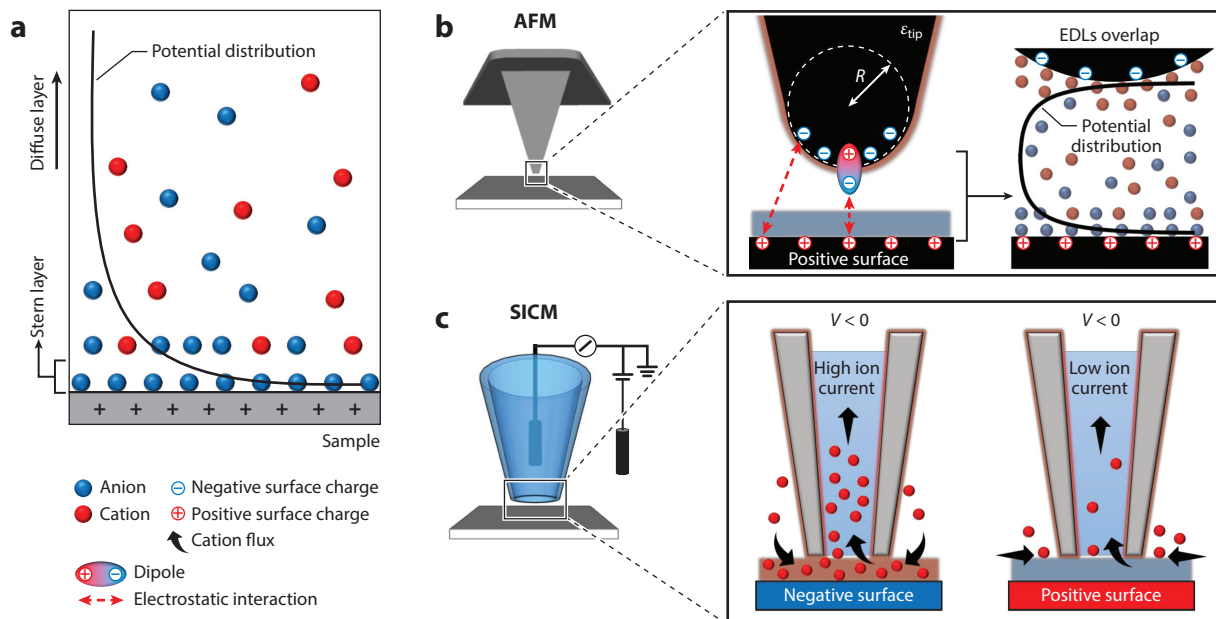


**Figure 1**

(a) Schematics of the EDL at a positively charged surface. (b) Scheme of the surface charge analysis using AFM. Surface charge measurements are based on the overlapping EDLs of the AFM probe and the sample. (c) Schematics of the surface charge analysis using SICM. Surface charge measurements are based on the voltage applied between the QRCEs and the concentration and flux of cations through the SICM probe (counter anions not shown).  $V < 0$  signifies negative tip bias. Abbreviations: AFM, atomic force microscopy; EDL, electrical double layer; QRCE, quasi-reference counter electrode; SICM, scanning ion conductance microscopy.

The GCS model accounts for ion size and hydration spheres for ions organized in the Stern layer (23, 32). The resulting potential and electric field in the double layer can be calculated from the charge density distribution and permittivity of the electrolyte using the nonlinear Poisson–Boltzmann equation (PBE) to describe the electric potential distribution normal to the charged surface (33–35). The electric potential and the local charge density decrease exponentially, as shown schematically in **Figure 1a**. For relatively dilute electrolyte solutions and moderate potentials, the GC model, which treats ions in the diffuse layer as point charges, is often reasonable (3), despite greatly underestimating the complexity of the EDL and simplifying the ion–ion interactions (3, 36, 37). Molecular dynamics simulations of the EDL are advancing apace and are useful to test elements of the GC and GCS models (38–40). In particular, constant potential molecular dynamics simulations reveal a wealth of information on ion and solvent adsorption and dynamics in the EDL, confirmed by experiments (41). However, such developments have yet to be incorporated into the analysis of AFM or SICM measurements, which tend to use the GC and GCS models or extensions thereof.

## DETECTION AND ANALYSIS OF SURFACE CHARGE IN ATOMIC FORCE MICROSCOPY AND SCANNING ION CONDUCTANCE MICROSCOPY EXPERIMENTS

AFM and SICM differ significantly in the nature of the probes, the probe–sample interaction (**Figure 1b,c**), and the resulting signals that are processed to obtain high-resolution topographical information, nanomechanical properties, and charge density (42, 43).

## Atomic Force Microscopy

AFM is one of the most used SPM techniques for measurements in ambient, liquid, or vacuum conditions. The AFM probe, a sharp tip or colloidal probe [e.g., for force spectroscopy (20, 44)] attached at the end of a cantilever, detects short- and long-range forces acting between the sample surface and the AFM probe.

When the probe approaches a surface immersed in solution, the experienced forces at the probe, in addition to electrostatic interaction (between EDLs), depend on hydrodynamic and van der Waals (VdW) interactions, which are also a function of the probe-surface distance (**Figure 1b**). Where the AFM probe is considered to be large (probe radius  $>20$  nm) (45), the probe-surface interaction can be treated as an ideal sphere-flat surface system. By deconvoluting the forces acting upon the AFM probe, the surface charge can be extracted. The Derjaguin, Landau, Verwey, and Overbeek (DLVO) theory (46) describes the surface charge contribution to the overall forces, whereby the model takes only attractive VdW forces and repulsive EDL forces into account (46), neglecting other interactions such as hydration forces, which become important at small probe-surface distances (e.g.,  $<2$  nm) (21).

The electrostatic force,  $F_{EDL}^{D \gg \lambda_D}$ , which results from the interaction of the AFM probe and substrate EDL, can be derived from the PBE using appropriate boundary conditions, assuming (a) the interaction between a flat surface and an AFM probe with a parabolic end with a curvature radius  $R$  and (b) a probe-surface distance ( $d$ ) much larger than  $\lambda_D$  ( $d \gg \lambda_D$ ):

$$F_{EDL}^{D \gg \lambda_D} = \frac{4\pi R \lambda_D \sigma_{\text{sample}} \sigma_{\text{tip}}}{\epsilon_r \epsilon_0} \exp\left(-\frac{d}{\lambda_D}\right), \quad 2.$$

where  $\sigma_{\text{sample}}$  and  $\sigma_{\text{tip}}$  are the surface charge density of the sample and the AFM probe, respectively.

The PBE is only valid when  $R$  is larger than  $\lambda_D$  (47). In addition, Equation 2 is only valid for low ionic strength, which usually excludes physiological ion concentrations (31). Despite these limitations and approximations, the electrostatic forces and surface charge density are still studied under the classical DLVO model (48–50). However, when  $d$  becomes smaller than 1–3 nm, the Stern layers (**Figure 1b**) start to overlap, resulting in repulsive, short-range entropic forces (solvation forces) (51). Consequently, the electrostatic interactions and the dielectric polarization of the AFM probe must be considered in the theoretical model. For instance, Zypman and coworkers (31) proposed an extended DLVO model, taking hydration forces and electrostatic interactions into account, which allowed measurements of the surface charge density in high electrolyte concentration in the snap-to-contact region (31).

One of the main challenges is related to the determination of the surface charge of the AFM probe, made of dielectrics such as silicon or silicon nitride, as the EDL of the AFM probe depends on the experimental conditions. To address this problem, symmetrical systems [probe and sample consist of the same material ( $\sigma_{\text{sample}} = \sigma_{\text{tip}}$ ) (52–55)] are used, and relative surface charge densities are analyzed (56) using either sharp AFM or colloidal probes; however, it should be noted that the achievable spatial resolution with colloidal probes is reduced.

For accurate analysis, the surface charge density of the AFM probe must be known by calibrating the AFM probe with a known sample, e.g., using gibbsite (57) or the tobacco mosaic virus (TMV) as a standard (58). Force-distance (FD) curves recorded on TMV resulted in stable surface charge density of the probe of  $8 \text{ mC m}^{-2}$  during the first 110 min immersed in  $0.01 \text{ mol L}^{-1}$  buffer solution.

Surface charges can also be mapped without a calibrated AFM probe using dynamic mode AFM, either intermittent mode (amplitude modulation or AM-AFM) (59) or noncontact mode (frequency modulation or FM-AFM) (60, 61), where the cantilever is driven to oscillation close to or at its resonance frequency and either the change of amplitude or the shift in frequency is

measured. FM-AFM measurements are usually performed in high-vacuum conditions providing atomic resolution, using stiff probes (e.g., tuning fork) (61). Recent developments enable FM-AFM in solution due to instrumental improvements (62–65), operating at higher ion concentrations (reducing the EDL length) and using small cantilever oscillations (63) to detect short-range interactions.

## Scanning Ion Conductance Microscopy

SICM uses a conical glass (typically borosilicate) or quartz nanopipette filled with an electrolyte solution. The ionic current that flows through the nanopipette orifice, with an applied bias between a quasi-reference counter electrode (QRCE) inside the nanopipette and a second QRCE placed in the bulk solution, creates a surface-sensitive feedback current (28, 66–68). The QRCEs are usually AgCl-coated silver wires, which have a stable potential under a variety of conditions (69). The ionic current is modified by the substrate presence, compared to when the nanopipette probe is in bulk solution, giving rise to a signal that depends on the topography (probe-substrate distance) and nature of the EDL at the charged interface (42, 67, 68), along with any other interfacial processes that change the local ionic composition (27, 70).

Depending on the pH of the aqueous solution, the silanol groups on the nanopipette walls will be more or less deprotonated, leading to negatively charged walls (71, 72). The resulting formation of a cation-selective region (EDL) inside the conical nanopipette (67, 73) means that cations are the majority charge carriers in this region (74, 75). This results in a nonlinear ion current-voltage response, widely termed ion current rectification (73), where the current magnitude at negative probe bias is higher than that at the equivalent positive probe bias. This diode-like behavior is dependent on a number of factors, including the charge on the pipette wall, the size of the nanopipette lumen compared to  $\lambda_D$  (ionic strength), and the nanopipette geometry. It may be further complicated by electroosmotic flow (EOF), which can be highly complex (76, 77). For these reasons, it is important that the geometry and properties of SICM nanopipettes are known and that detailed mass transport modeling of the nanopipette is undertaken (76, 78, 79).

When the SICM probe is positioned close to a charged interface, the interface will also contribute the perm-selectivity and mass transport properties of the nanopipette-surface configuration, and thus the current response results from surface-induced ion current rectification (25, 27, 28, 80); this is exemplified with the simple schematic shown in **Figure 1c** (28).

The ionic flux at the nanopipette opening is described by the Nernst–Planck equation that considers ion diffusion, migration, and EOF (when applicable). The electric potential across the solution, which depends on the space charge distribution, is described by the Poisson equation, and the entire SICM current response can be modeled by coupling the equations into the Poisson–Nernst–Planck equation. Solution velocity due to EOF (which is integrated in the Nernst–Planck equation) can often be neglected if the surface charge density at the nanopipette wall and substrate is low (18, 28, 81), but it needs to be taken into account at higher charge density (71, 82). Models of SICM mass transport and the resulting current response have developed apace since the original finite element method (FEM) simulations (83, 84). Inclusion of EOF in FEM models can be computationally expensive, but if pixel-level self-referencing methods are used (see below), where the quantity of interest is the current ratio with the probe near the surface and in bulk solution, simulations for these two situations can often ignore EOF, with little loss of accuracy in the resulting current ratio (67).

Numerical simulations for surface charge density calculations have been used for both AFM and SICM (22, 25, 85). For SICM, this is commonly based on FEM analyses (25), which are capable of simulating length scale domains that are within the GCS model or EDL-related models.

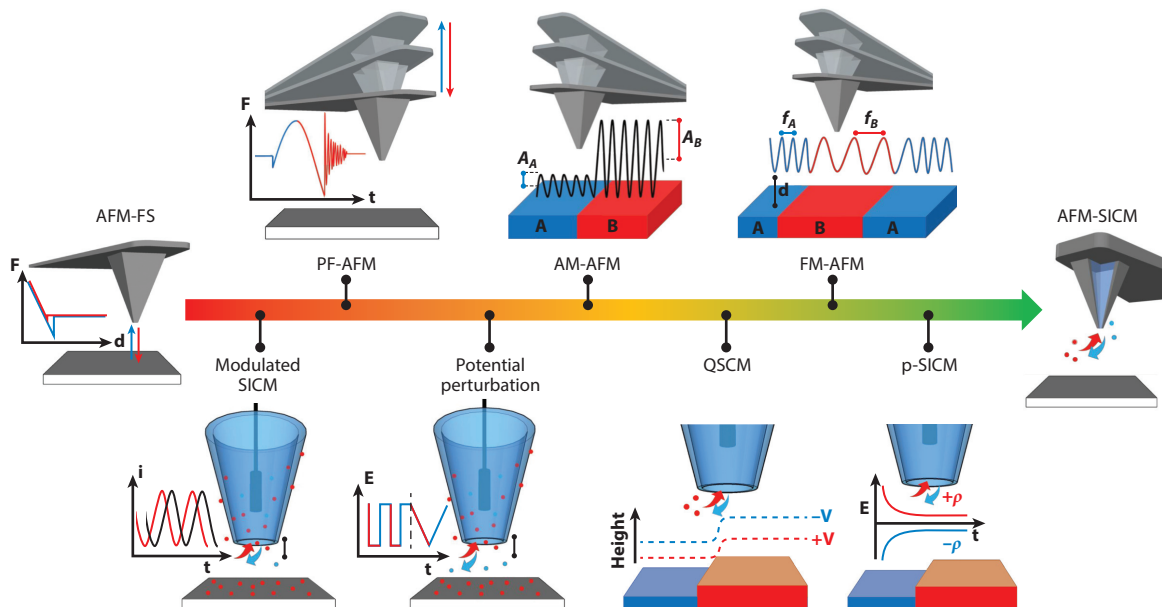


**Figure 2**

Atomic force microscopy (AFM) and scanning ion conductance microscopy (SICM)-based methods developed over the years to study surface charges in solution. These methods include AFM-force spectroscopy (AFM-FS), pulsed force (PF)-AFM, amplitude modulation (AM)-AFM, frequency modulation (FM)-AFM, modulated SICM, potential perturbation SICM, quantitative surface conductance microscopy (QSCM)-SICM, potentiometric (p)-SICM, and hybrid AFM-SICM.

It is important that the simulation domain geometry and boundary conditions are in line with the experimental framework. For quantitative analyses, several simulation approaches are used to construct a working curve that can convert experimental data into surface charge values as shown for various substrates (18, 25–28, 50, 71, 83, 85).

For AFM, due to the complex probe-substrate force interactions, the selection of the theoretical model strictly depends on the experimental conditions and the used AFM mode. Although FEM simulations have also been utilized to determine the surface charge density (85), density functional theory (DFT) calculations (22, 86, 87) and molecular dynamics simulations are more widely used.

## ATOMIC FORCE MICROSCOPY AND SCANNING ION CONDUCTANCE MICROSCOPY STRATEGIES FOR CHARGE MAPPING

Since the study of electrified solid-liquid interfaces was pioneered by Butt (20), AFM has evolved as a tool for measuring local interfacial forces, e.g., for testing the DLVO theory (53, 56, 88). In contrast, following the initial introduction of SICM by Hansma et al. (66), there was little interest in SICM until Korchev and coworkers introduced a more robust constant distance imaging mode (89). In this section, we briefly discuss the major developments of AFM and SICM methodology for the investigation of charged solid-liquid interfaces (Figure 2).

### Atomic Force Microscopy Charge Mapping

AFM has a long-standing history for studying charged interfaces (20, 44, 53, 90–92). One of the advantages of AFM is its versatility in terms of operational modes. For example, FD curves (20) can be recorded in both static and dynamic modes (87) as the basis for statistical analysis.

Topographical, electrical, and nanomechanical properties can be imaged simultaneously at reasonable imaging times using dynamic mode AFM (22, 85, 93, 94).

AFM-force spectroscopy (AFM-FS) studies of the double layer at the solid-liquid interface were pioneered by Pashley's group (44) and Butt (20). Analyzing FD curves with respect to the DLVO theory enabled the determination of interfacial charge properties of electrodes (90, 95, 96), semiconductors (91), polymers (97, 98), and biological samples (49, 50, 99).

Recording FD curves at a two-dimensional grid of points using either static or dynamic mode [force-volume (FV)-AFM] results in, e.g., surface charge maps (47, 87, 100); however, this mode may suffer from long acquisition times. In contrast, pulsed force (PF)-AFM mode (101), where the cantilever oscillates with an amplitude of 20–500 nm at a frequency far below the resonance frequency (100 Hz to 2 kHz), maps at scan velocities comparable to contact mode AFM while the nanomechanical and electrical properties are recorded (93). Marti, Fujihira, and colleagues (93, 102) demonstrated the first application of PF-AFM for surface charge mapping by oscillating the cantilever in solution in the noncontact regime for mapping double layer forces of, e.g., a mixed  $\text{Al}_2\text{O}_3$ ,  $\text{SiO}_2$  surface with a resolution of tens of nanometers (93).

The spatial resolution has been significantly improved using dynamic AFM modes, i.e., using methods derived from FM-AFM (85, 94, 103, 104) and AM-AFM (87, 105). In FM-AFM-based techniques, the frequency shift of the cantilever is proportional to the double layer force gradient and thus to the dielectric properties of the surface (94, 106). For example, using cantilevers with small force constants ( $\sim 0.3 \text{ N m}^{-1}$ ) at high frequency modulation, researchers recorded high-resolution images of the dielectric properties of Si and  $\text{SiO}_2$  substrates (85). Furthermore, working in the range of megahertz frequencies (higher than the dielectric relaxation frequency of the electrolytic solution) and scanning the surface at a distance larger than  $\lambda_D$  ( $\sim 10 \text{ nm}$  in 1 mM monovalent electrolyte solutions), the frequency changes as a function of the electrostatic forces can be mapped (30, 85). Stiffer cantilevers ( $\sim 40 \text{ N m}^{-1}$ ) in combination with an alternating current (AC) bias voltage in the kilohertz regime have been used for simultaneous imaging of the surface structure and the potential distribution at solid-liquid interfaces (94).

Recently, Garcia and coworkers (107) introduced bimodal force microscopy [three-dimensional (3D)-AFM], which is derived from AM-AFM and uses multifrequency excitation and multicomponent signal processing. 3D-AFM has been demonstrated to give atomic resolution of solid-liquid interfaces of hydrophobic and hydrophilic surfaces, such as mica, graphite, and graphene, and biological samples such as DNA, proteins, and lipid bilayers (22).

## Scanning Ion Conductance Microscopy Charge Mapping

The inspiration for SICM charge mapping came from initial observations that substrate surface charge could affect the ion current in SICM (25, 80, 108). It is now widely recognized that surface charge effects can be important in SICM topographical imaging protocols (109).

The first SICM experiments that deconvoluted surface charge and topography (25) utilized a hopping mode protocol in which the nanopipette probe was approached toward the surface at a series of pixels, with a small  $z$ -distance modulation (a few hundred hertz), while applying a fixed direct current (DC) bias between the QCREs. The surface was mapped through a change in the amplitude of the AC response due to the positional modulation (using a lock-in amplifier); both the AC phase and DC ionic current were shown to be sensitive indicators of surface charge.

These studies (25) and others (110, 111) highlighted that (earlier) topographical SICM imaging could be convoluted by surface charge effects, prompting the search for further protocols whereby the topography and surface charge could be detected independently. The introduction of bias modulation SICM (112), in which a harmonic oscillation of the SICM bias (at frequencies up to

30 kHz) was applied around a net bias of zero, facilitated topographical mapping, free from any surface charge effects, using both the phase (between ca. 100 Hz and 30 kHz oscillation frequency) and amplitude (up to ca. 500 Hz oscillation frequency) of the resulting AC current for positional feedback. Then, with an applied bias at the same probe position, e.g., by sweeping the potential linearly or triangularly, the ion conductance current became more surface charge sensitive (27). The development of a detailed model of the SICM response facilitated quantitative surface charge mapping, including of living cells under physiological conditions (28).

To speed up surface charge mapping by a factor of 10, a faster hopping-potential pulse DC mode was introduced (26), in which the nanopipette probe was approached quickly from bulk solution to the surface (at each pixel) with a very small applied bias. The SICM current response essentially detected only the surface topography (DC set point), and at the set point distance the bias was then pulsed to a large value (a magnitude of several hundred millivolts, with the polarity selected depending on the surface charge) for a brief period, where the current-time curve was surface charge (EDL) sensitive. The same potential pulse protocol was applied in bulk, at each pixel, to self-reference the surface signal before the probe was translated to the next point where the protocol was repeated. This method was shown to be capable of readily detecting surface charge on living cells under physiological buffer conditions.

A technique called quantitative surface conductivity microscopy uses the surface charge artifacts in SICM topographical images for quantification (113). The topography is mapped in two consecutive scans, one with a positive bias (+100 mV) and one with a negative bias (−100 mV), with the same set point. Differences in the topography, found by subtracting one image from the other, are analyzed to obtain quantitative charge maps. This method uses DC imaging, as employed in the original SICM studies (66), requiring that the two QRCEs maintain a stable potential throughout the scan. As this method analyzes small differences in topography between two maps, the  $z$ -piezo noise and thermal drift between scans need to be minimized (114). The technique has been used to obtain detailed surface charge maps on supported lipid bilayers (113, 115) and self-assembled DNA structures (116).

An intuitive approach to SICM charge mapping, again based on a self-referencing hopping mode, is to measure the absolute value of the ratio of the ion currents at applied negative and positive nanopipette bias, termed the rectification ratio (29). Here, the probe, at a fixed DC bias, is translated to the surface to sense the near surface from a specific current change, and with the nanopipette in that position, a staircase ramp through the potentials (e.g., −0.6 V to +0.6 V) is applied, while measuring the current-time response after each step (29). As with triangular potential perturbation measurements, the current response (and hence current ratio) at the most extreme potentials is most sensitive to surface charge.

SICM current-potential curves during a triangular sweep of the potential, obtained with the probe near a charged surface and in bulk solution, have been analyzed in detail to reveal a hysteresis crossing point,  $V_{cp}$ , between the forward and reverse scan curves (117). The change in  $V_{cp}$  between the bulk and near surface correlated with the classical GC model, allowing local surface potential measurements to be made without knowledge of probe geometry or modeling (117, 118).

A further SICM method exploring the charge-topography convolution in SICM images uses fast nanopipette approach rates in a hopping mode and the analysis of the current response to reveal a surface charge density contrast map (119). At the high approach rates ( $85 \mu\text{m s}^{-1}$ ) an overshoot in the  $z$ -piezo movement and corresponding current change is observed, which is strongly dependent on the surface charge.

Because surface charge is related to the surface potential (120, 121), potentiometric SICM (p-SICM) is an important development (122, 123) that makes use of a dual-channel (theta) nanopipette, with one channel recording the topography in DC hopping mode while the other

measures the open circuit potential during scanning, from which near-surface potential maps can be obtained (110, 121–123), as shown for several samples (120, 121).

## FluidFM

A novel strategy for SPM-based charge measurements is FluidFM (**Figure 2**), which has been developed to simultaneously and independently resolve surface charge distribution and topography, combining the fast vertical, accurate positioning of the AFM probe and the ion sensing of SICM, building on the strengths of both techniques (24). FluidFM consists of a hollow AFM tip-cantilever with an open channel (diameter of 300 nm) filled with an electrolyte solution. FluidFM is capable of charge mapping with similar sensitivity to SICM, while relying on the robust topography feedback of AFM. The current trade-off of this technique is that the ion conductance channel opening (the ion-sensitive part of the probe) is still comparatively larger than AFM and SICM probes, limiting its spatial resolution. Although this is an engineering challenge, smaller FluidFM probes might be seen in the future.

## IMAGING APPLICATIONS

To date, AFM and SICM have been employed to map the local surface charge density of model substrates such as mica and silicon (25, 54, 85, 124, 125), inorganic substrates (25, 57, 126–128), polymers (26, 129), and biological samples (28, 30, 58, 106, 113, 115, 116, 130), as illustrated in **Supplemental Figure 1**.

Supplemental Material >

## Materials Science and Electrochemistry

The surface charge of polymers, electrodes, glass, and ceramics has been investigated by SICM (71, 125, 131) and AFM (85, 91, 93, 96, 103, 132). For electrode materials and nanocarbon materials such as graphene, knowledge of heterogeneities in surface charge distribution is important to understand local structure-activity relationships (133, 134). Strelcov et al. (132) developed vacuum-compatible electrolytic cells using microchannel array technology for studying the EDL potential at the graphene-electrolyte interface using Kelvin probe force microscopy, which was operated under vacuum, yet after different electrolytic conditions. The water-graphene interface has been investigated with FM-AFM and 3D-AFM, elucidating the interfacial water distribution on graphene and probing the formation of hydration layers in the range of 0.3–0.6 nm (135). Open-loop electric potential microscopy (3D-OL-EPM), which is based on applying a high frequency AC voltage between the AFM probe and sample to map accumulated charges and Z potential profiles at the electrode-electrolyte interface, has been demonstrated for polarizable (gold and platinum) and nonpolarizable (copper) electrodes as a function of the applied voltage (136). By applying an anodic potential, gold and platinum electrodes showed EDLs with accumulations of negative charges, whereas copper electrodes exhibited positive charges at the electrode-electrolyte interface.

There have been attempts to correlate surface charge from SICM and catalytic activity for the simple redox process of  $\text{Fe}(\text{CN})_6^{4-/3-}$  at modified highly oriented pyrolytic graphite (HOPG). Surface defects, induced by Ar plasma treatment, were found to have a higher surface charge that was correlated to faster electron transfer kinetics. The more extensive the plasma treatment, the closer were the electron transfer kinetics to reversible behavior, and unmodified surfaces showed the slowest kinetics (125). However, this electrochemical process is sensitive to rapid surface aging and/or contamination of the HOPG surface. Surfaces studied immediately after cleavage show reversible kinetics on the typical voltammetric timescale (137), but the electron transfer kinetics

deteriorate with time after HOPG cleavage (137, 138). Such effects need to be considered when designing studies with HOPG (139).

SICM has been configured with a carbon fiber microelectrode substrate to measure the delivery of electroactive species (charged and uncharged) from a nanopipette, revealing the importance of local electrode surface charge in influencing the delivery process (131, 140), with complex EOF patterns observed under some conditions (71). This configuration was further adapted to make an artificial synapse, in which the SICM delivered rapid pulses of neurotransmitter (dopamine) on demand at >1,000 different locations of a carbon fiber microelectrode in a single experiment (141). Variations in spatiotemporal electrochemical activity were related to heterogeneities in the surface charge of the microelectrode.

Biopolymers, such as cellulose-modified surfaces, have been studied with colloidal-based AFM-FS, revealing that surface charge density affects bacterial adhesion (129). Cellulose-modified surfaces, treated with antimicrobial agents, exhibited different degrees of antimicrobial activity, depending on the surface charge of the film. The double layer forces of polymer-electrolyte interfaces of electro-active polymers have also been studied (96–98).

For SICM, polymeric surfaces have mostly been used as test samples for visualizing surface charge (25, 26, 29), although the transport of ions within polymeric surfaces can be assessed (126).

## Mineralogy

Initially, AFM charge mapping in mineralogy has been focused on studies of model substrates such as mica and clay minerals (22, 57, 87, 142). The surface charge density of kaolinite [triclinic  $\text{Al}_2\text{Si}_2\text{O}_5(\text{OH})_4$ ] nanoparticles exposed to different electrolyte solutions and pH values has been mapped achieving a lateral resolution of 10 nm (87). The surface charge density was quantitatively extracted by fitting the FD curves with the DLVO model. The effect of  $\text{CaCl}_2$  in solution on the surface charge of kaolinite indicated that the surface charge was dependent on the salinity of the medium, showing a small increase with an increase of the salt concentration up to 10 mM and a decrease with higher concentrations (50 mM) of  $\text{CaCl}_2$ . The increase of the surface charge at low salt concentration was explained by the adsorption of calcium ions, while the decrease at higher concentration is due to the adsorption of chloride ions, which was supported by DFT calculations (87).

The electrostatic and hydration forces of semiconducting faceted nanoparticles of  $\text{SrTiO}_3$  have been recently studied as function of the pH, which is important, e.g., in photocatalysis (105). First, the topography was recorded with AM-AFM, and in a second step, the surface charge was mapped using FV-AFM (dual pass). It was shown that the surface charge depends on the nanoparticle facet. The squared {100} facets have more positive charge than the hexagonal {110} facets. It has been also shown that both facets reverse their charge with a decrease of the pH and reach the isoelectric point at different values of pH (6 for {100} facets and 4 for {110} facets).

In a series of publications, Garcia and coworkers (22, 143, 144) have demonstrated the potential of 3D-AFM for imaging of solid-liquid interfaces with high force (piconewton), sufficient time (seconds), and high spatial (atomic) resolution. For example, the organization of solvent molecules and ions at solid-liquid hydrophilic (mica) and hydrophobic (hexagonal boron nitride) interfaces have been studied, revealing that traces of airborne and waterborne hydrocarbon molecules at the hydrophobic substrate are responsible for the formation of the hydration layer (144). Combining 3D-AFM with molecular dynamics simulations at mica samples, the authors emphasize the importance of the charge density of the AFM tip to obtain reliable data on charge density (sample) (22). Neutral AFM probes provide information on total particle distribution (water and ions) and charged probes give access to the charge density distribution (**Figure 3a**).

Downloaded from [www.annualreviews.org](http://www.annualreviews.org).

Guest (guest)

IP: 3.133.12.172

On: Sun, 05 May 2024 04:37:44

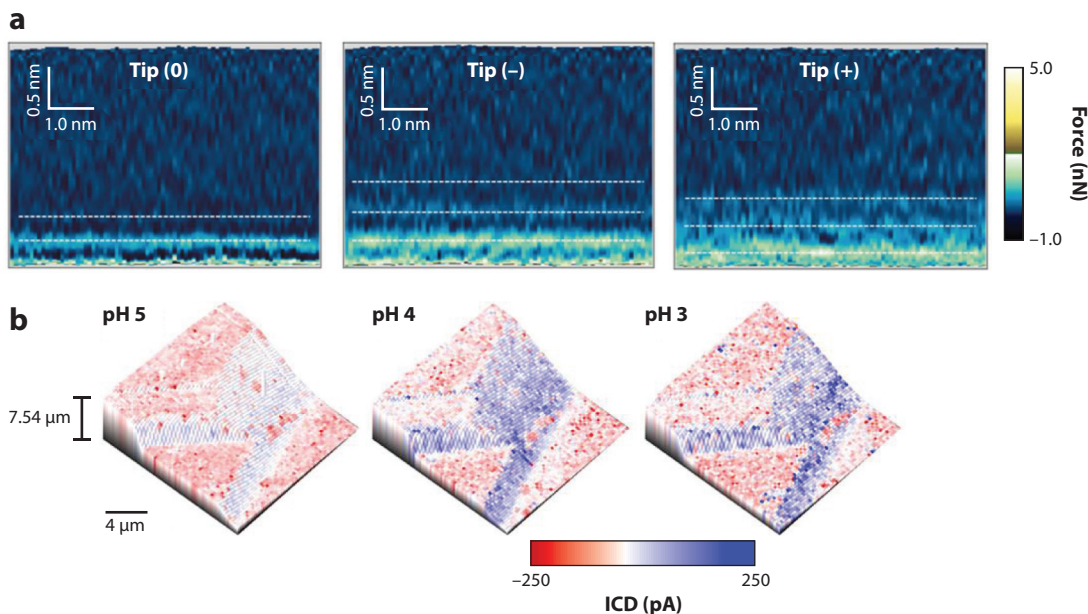


**Figure 3**

(a) Two-dimensional ( $x, Z$ ) force maps for a 1 M NaCl solution close to a mica surface, recorded using neutral, negative, and positive AFM probes. Panel adapted with permission from Reference 22; copyright 2021 American Physical Society. (b) Combined topography and ICD images of a dickite crystal at pH 5, 4, and 3 recorded using self-referencing SICM. Panel adapted with permission from Reference 145; copyright 2021 American Chemical Society. Abbreviations: AFM, atomic force microscopy; ICD, ion current difference; SICM, scanning ion conductance microscopy.

Most recently, the surface charge of dickite crystals [monoclinic  $\text{Al}_2\text{Si}_2\text{O}_5(\text{OH})_4$ ] was mapped by SICM by recording ion current-voltage curves at each pixel (145). Surface charge was represented as an ion current difference, which is calculated as the sum of the normalized (to bulk) ion current rectification values at the most extreme negative and positive potentials. The ion current difference sign follows that of the surface charge, providing a direct charge contrast visualization. As shown in **Figure 3b**, while dickite always exhibits a negative charge independent of the pH (pH 3, pH 4 and pH 5), the edges carried a pH-dependent positive charge, with the charge density increasing with acid concentration. It was also shown that the surface charge was affected by the presence of malonate in the bulk solution, probably due to the dissolution of siloxane and gibbsite-like layers favored by the malonate.

## Life Sciences

Both AFM and SICM are highly suitable to study biological samples, such as nucleic acids (100, 106, 116, 146), proteins (49, 147), lipids (113, 115), chromosomes (148), viruses (58, 99), and living cells (18, 26, 28, 30, 81, 119, 149), as measurements can be made in buffered solution. Surface charge and electrical properties are characteristics related to the biochemical functions and interactions of biological samples, influencing, e.g., antibody-antigen, cell-drug and cell-virus interactions, enzymatic reactions, cell adhesion, and DNA condensation. The recognition between host cells and viruses is governed by specific and nonspecific interactions, and a contribution of the latter is produced by the electrostatic forces, which depend on the surface charge of the viruses

(99), whereas the surface charge is a unique feature of viruses that strongly depends on the nature of the viral capsid, as shown in recent AFM studies (99).

AFM-FS was used to study the surface charge distribution of living bacteria at indium tin oxide substrates under physiological conditions (30). The surface charge was obtained by analyzing the regions of the FD curves where the cantilever's deflection was constant, i.e., at a probe-sample separation larger than 10 nm. In this region, the deflection depends on the surface tension and thus, indirectly on the variation of the surface charge density. Images of the cell wall charge distribution of Gram-positive bacteria (*Rhodococcus wratislaviensis*) (30) reveal small charge heterogeneities, in which local charge reductions are visible. These negative spots correlated with a lack of teichoic acids (anionic polymers characteristic of Gram-positive bacteria) at such spots (30).

FM-AFM has been used to study the electrical and conformational properties of DNA in electrolytic solutions (106, 146). Under high ionic concentration conditions, the more stable right-handed helical DNA conformation (B-DNA) can change into the left-handed helical DNA conformation (Z-DNA). This transition leads to a reorganization of the nucleobases and thus to a change of the surface charge of the DNA. Kominami et al. (146) performed measurements at B-Z-B DNA multiconformational molecules in a 0.05 mol L<sup>-1</sup> nickel (II) chloride solution. The frequency shift map was converted into a 3D FD curve map using Sader's method (150) and fitted to the DLVO model. The obtained high-resolution surface charge density map is depicted in **Figure 4a**. **Figure 4b** shows the surface charge profile along the DNA that illustrates the different surface charge of B-DNA and Z-DNA with the B-Z junction.

SICM is very suitable for surface charge-topography mapping of living cells (42, 67). The first studies of this type (28) revealed that *Zea mays* root hair cells have high negative surface charge at their tips. Adipocyte cells are responsible for the storage and regulation of lipids in mammalian systems; distinct surface charge distributions were detected under physiological conditions, including positively charged domains that were tentatively ascribed to the possible locations of fatty acid transporters.

Living PC-12 cells (26), cultured to be neuron-like, were investigated with the fast self-referencing potential-pulse mode described above. The surface charge of cancer cells (HeLa) has also been investigated under the influence of membrane-thinning agents, such as dimethyl sulfide (119). The resulting increase in image resolution allowed detailed and quantitative surface charge-topography visualization and the detection of subtle variations and heterogeneities in surface charge. To illustrate the versatility of the biorelated samples that are amenable to surface charge mapping, a study of human hair (18) subjected to different treatments reveals the power of SICM for quantitative measurements.

Surface charge mapping of live bacteria cells showed considerable differences between the ionic environment of Gram-negative (*Escherichia coli*) and Gram-positive (*Bacillus subtilis*) bacteria (81), with the bioelectrical environment of *B. subtilis* found to be considerably more negatively charged compared to *E. coli*. SICM was able to detect surface charge heterogeneities within individual bacteria and also between different bacteria. The effective surface charge on *B. subtilis* was in the range of -350 and -450 mC m<sup>-2</sup> using a simple GCS model. To determine how the cell wall structure could influence the SICM current response, a more detailed model was developed and parametrized with known bacterial properties, demonstrating that the cell wall ion permeability is an important contributor to the SICM current response. **Figure 4c** depicts regions of higher negative charge near *B. subtilis*, not detected in the topographical images (**Figure 4d**), which are attributed to extracellular polymeric substances produced by the cells (81).

Charge mappings of lipid bilayers using AFM date back two decades, when force maps in low ionic concentrations were recorded (56). Recent SICM studies of surface charge at lipid bilayers

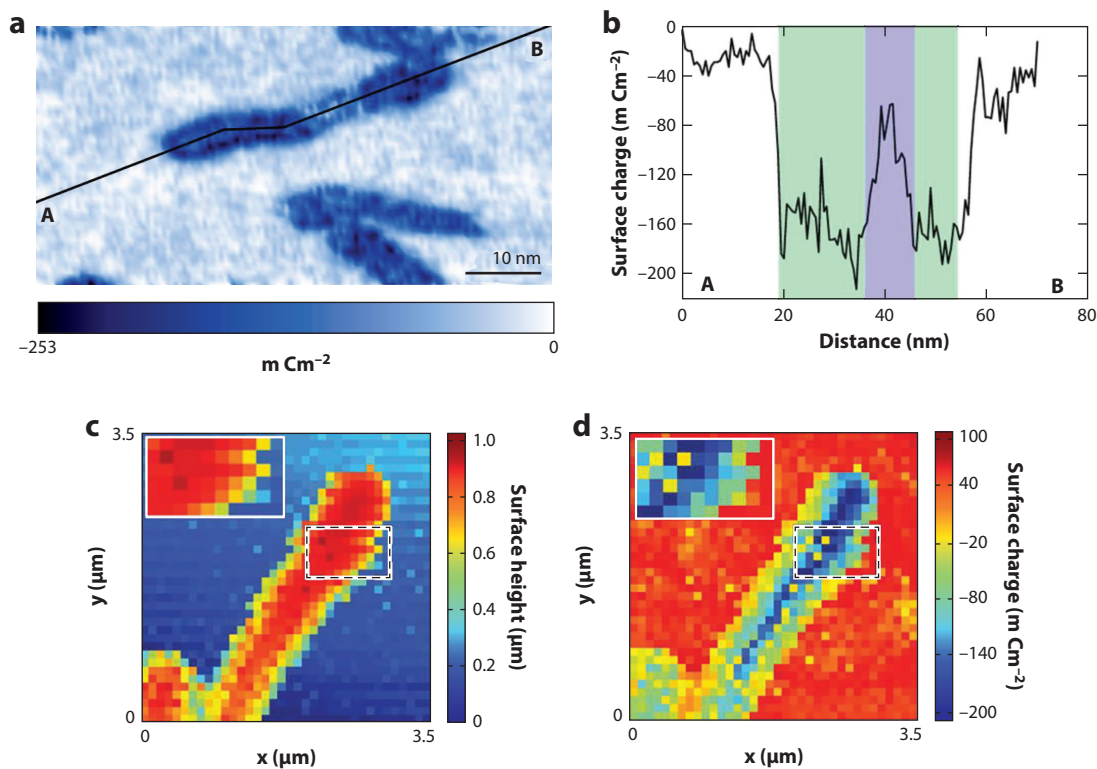


**Figure 4**

(a) Surface charge density map of B-Z-B DNA obtained by FM-AFM and (b) surface charge profile along the A-B polyline in panel a. The green area corresponds to the B-DNA and the blue area to the Z-DNA conformation. Panels a and b adapted with permission from Reference 146. (c) SICM topography and (d) surface charge of *Escherichia coli* acquired simultaneously. Panels c and d adapted with permission from Reference 81; copyright 2020 American Chemical Society. Abbreviations: B-DNA, right-handed helical DNA conformation; FM-AFM, frequency modulation atomic force microscopy; SICM, scanning ion conductance microscopy; Z-DNA, left-handed helical DNA conformation.

showed inherent charge of the lipid species present in different domains (113, 115). Surface charge of DNA origami nanostructures deposited on mica demonstrated surface charge density quantification down to the single molecule and revealed that the surface charge density of mica can be altered with binding of divalent ions (116).

**Supplemental Tables 1 and 2** present summaries of surface charge density studies conducted in the last two decades using AFM and SICM.

**Supplemental Material** >

## CONCLUSION AND PERSPECTIVE

The distribution of surface charges at the material/electrolyte interface is of fundamental importance for understanding interfacial processes and can be studied with AFM and SICM, as highlighted in this review. The probe size is an important factor for both techniques, because spatial resolution, and to an extent the ability to resolve local surface charge, is limited by the size of the probe. AFM probes with a nominal radius smaller than 5 nm are commercially available and allow high-resolution imaging of topography and surface charge. However, for surface charge mappings, the size of AFM probes must be carefully selected, depending on the theoretical model

used. For the classical DLVO model, the nominal radius must be larger than that of the Debye length of the system under study and, colloidal probes, although limited in resolution, are frequently used for such measurements. An advantage of AFM for the study of solid-liquid interfaces is the number of static and dynamic modes available, which allow the acquisition of images with atomic resolution in solution in combination with FEM, DFT, and molecular dynamics simulation and well-established statistical data analysis.

SICM probes used for surface charge mapping typically have an orifice diameter of 60–200 nm, as there is a need to balance the response of the nanopipette, which is ion current rectifying, with the contribution from the surface. Nanopipettes with a diameter of 10 nm have been recently prepared (151) but not yet used for SICM. Further improvements to SICM scanning protocols, which are yet to be employed for charge mapping, have significantly decreased scan times to a couple of minutes for a 70- $\mu\text{m}^2$  scanned area (152), affording a new dimension (temporal) to SICM measurements.

The better understanding of the EDL structure afforded by molecular dynamics simulations is a promising way to create reliable descriptors of the double layer, which have been used to improve models. These implementations will improve charge mapping accuracy and expand SPM applications beyond surface charge visualization and into probing the EDL composition, structure, and properties by accurately modeling the experimental response.

## DISCLOSURE STATEMENT

The authors are not aware of any affiliations, memberships, funding, or financial holdings that might be perceived as affecting the objectivity of this review.

## ACKNOWLEDGMENTS

This work is part of the Break Biofilm project that has received funding from the European Union's 2020 research and innovation program under Marie Skłodowska Curie grant agreement 813439. P.R.U. thanks the Royal Society for a Wolfson Research Merit Award.

## LITERATURE CITED

1. Trefalt G, Ruiz-Cabello FJM, Borkovec M. 2014. Interaction forces, heteroaggregation, and deposition involving charged colloidal particles. *J. Phys. Chem. B* 118(23):6346–55
2. Metwally S, Stachewicz U. 2019. Surface potential and charges impact on cell responses on biomaterials for medical applications. *Mater. Sci. Eng. C* 104:109883
3. Gonella G, Backus EHG, Nagata Y, Bonthuis DJ, Loche P, et al. 2021. Water at charged interfaces. *Nat. Rev. Chem.* 5(7):466–85
4. Bard AJ, Faulkner LR. 2001. *Electrochemical Methods*. New York: John Wiley & Sons. 2nd ed.
5. Hunter RJ. 1988. *Zeta Potential in Colloid Science: Principles and Applications*. London: Elsevier. 3rd ed.
6. Grahame DC. 1947. The electrical double layer and the theory of electrocapillarity. *Chem. Rev.* 41(3):441–501
7. Szekeres M, Tombácz E. 2012. Surface charge characterization of metal oxides by potentiometric acid-base titration, revisited theory and experiment. *Colloids Surf. A Physicochem. Eng. Asp.* 414:302–13
8. Nam K-M, Chang B-Y. 2014. Electrochemical impedance method to measure the potential of the outer Helmholtz plane. *J. Electrochem. Soc.* 161(6):H379–83
9. Williams DJA, Williams KP. 1978. Electrophoresis and zeta potential of kaolinite. *J. Colloid Interface Sci.* 65(1):79–87
10. Israelachvili J, Min Y, Akbulut M, Alig A, Carver G, et al. 2010. Recent advances in the surface forces apparatus (SFA) technique. *Rep. Prog. Phys.* 73(3):036601

11. Ouyang L, Shaik R, Xu R, Zhang G, Zhe J. 2021. Mapping surface charge distribution of single-cell via charged nanoparticle. *Cells* 10(6):1519
12. Nishino M, Matsuzaki I, Musangil FY, Takahashi Y, Iwahashi Y, et al. 2020. Measurement and visualization of cell membrane surface charge in fixed cultured cells related with cell morphology. *PLOS ONE* 15(7):e0236373
13. Wu F, Zhou B, Wang J, Zhong M, Das A, et al. 2019. Photoelectrochemical imaging system for the mapping of cell surface charges. *Anal. Chem.* 91(9):5896–903
14. Decker R, Wang Y, Brar VW, Regan W, Tsai H-Z, et al. 2011. Local electronic properties of graphene on a BN substrate via scanning tunneling microscopy. *Nano Lett.* 11(6):2291–95
15. Yoo MJ, Fulton TA, Hess HF, Willett RL, Dunkleberger LN, et al. 1997. Scanning single-electron transistor microscopy: imaging individual charges. *Science* 276(5312):579–82
16. Ye S, Yan X, Husain MK, Saito S, De Groot CH, Tsuchiya Y. 2021. Direct observation of surface charge redistribution in active nanoscale conducting channels by Kelvin Probe Force Microscopy. *Nanotechnology* 32(32):325206
17. Araki K, Le Y, Aso Y, Ohoyama H, Matsumoto T. 2019. Time-resolved electrostatic force microscopy using tip-synchronized charge generation with pulsed laser excitation. *Commun. Phys.* 2(1):10
18. Maddar FM, Perry D, Brooks R, Page A, Unwin PR. 2019. Nanoscale surface charge visualization of human hair. *Anal. Chem.* 91(7):4632–39
19. Happel P, Thatenhorst D, Dietzel ID. 2012. Scanning ion conductance microscopy for studying biological samples. *Sensors* 12(11):14983–88
20. Butt H-J. 1991. Measuring electrostatic, van der Waals, and hydration forces in electrolyte solutions with an atomic force microscope. *Biophys. J.* 60(6):1438–44
21. Jarmusik KE, Eppell SJ, Lacks DJ, Zypman FR. 2011. Obtaining charge distributions on geometrically generic nanostructures using scanning force microscopy. *Langmuir* 27(5):1803–10
22. Benaglia S, Uhlig MR, Hernández-Muñoz J, Chacón E, Tarazona P, Garcia R. 2021. Tip charge dependence of three-dimensional AFM mapping of concentrated ionic solutions. *Phys. Rev. Lett.* 127(19):196101
23. Schmickler W. 2009. Electrochemical theory: double layer. In *Encyclopedia of Electrochemical Power Sources*, ed. J Garce, pp. 8–13. Amsterdam: Elsevier
24. Dorwling-Carter L, Aramesh M, Han H, Zambelli T, Momotenko D. 2018. Combined ion conductance and atomic force microscope for fast simultaneous topographical and surface charge imaging. *Anal. Chem.* 90(19):11453–60
25. McKelvey K, Kinneer SL, Perry D, Momotenko D, Unwin PR. 2014. Surface charge mapping with a nanopipette. *J. Am. Chem. Soc.* 136(39):13735–44
26. Page A, Perry D, Young P, Mitchell D, Frenguelli BG, Unwin PR. 2016. Fast nanoscale surface charge mapping with pulsed-potential scanning ion conductance microscopy. *Anal. Chem.* 88(22):10854–59
27. Perry D, Al Botros R, Momotenko D, Kinneer SL, Unwin PR. 2015. Simultaneous nanoscale surface charge and topographical mapping. *ACS Nano* 9(7):7266–76
28. Perry D, Nadappuram BP, Momotenko D, Voyias PD, Page A, et al. 2016. Surface charge visualization at viable living cells. *J. Am. Chem. Soc.* 138(9):3152–60
29. Zhu C, Zhou L, Choi M, Baker LA. 2018. Mapping surface charge of individual microdomains with scanning ion conductance microscopy. *ChemElectroChem* 5(20):2986–90
30. Marlière C, Dhahri S. 2015. An in vivo study of electrical charge distribution on the bacterial cell wall by atomic force microscopy in vibrating force mode. *Nanoscale* 7(19):8843–57
31. Li L, Eppell SJ, Zypman FR. 2020. Method to quantify nanoscale surface charge in liquid with atomic force microscopy. *Langmuir* 36(15):4123–34
32. Stumm W, Morgan JJ. 1996. *Aquatic Chemistry: Chemical Equilibria and Rates in Natural Waters*. New York: John Wiley & Sons. 3rd ed.
33. Hiemenz PC, Rajagopalan R, eds. 1997. *Principles of Colloid and Surface Chemistry*. Boca Raton, FL: CRC Press. 3rd ed.
34. Schmickler W, Santos E. 2010. *Interfacial Electrochemistry*. Berlin: Springer Sci. Bus. Media. 2nd ed.
35. Henderson D, Boda D. 2009. Insights from theory and simulation on the electrical double layer. *Phys. Chem. Chem. Phys.* 11(20):3822–30

Downloaded from www.annualreviews.org.

Guest (guest)

www.annualreviews.org • Surface Charge Density in Aqueous Solution 261

On: Sun, 05 May 2024 04:37:44

36. Gschwend GC, Olaya A, Girault HH. 2020. How to polarise an interface with ions: the discrete Helmholtz model. *Chem. Sci.* 11(39):10807–13
37. Groß A, Sakong S. 2019. Modelling the electric double layer at electrode/electrolyte interfaces. *Curr. Opin. Electrochem.* 14:1–6
38. Brown MA, Bossa GV, May S. 2015. Emergence of a Stern layer from the incorporation of hydration interactions into the Gouy–Chapman model of the electrical double layer. *Langmuir* 31(42):11477–83
39. Yi M, Nymeyer H, Zhou H-X. 2008. Test of the Gouy–Chapman theory for a charged lipid membrane against explicit-solvent molecular dynamics simulations. *Phys. Rev. Lett.* 101(3):038103
40. Dewan S, Carnevale V, Bankura A, Eftekhari-Bafrooei A, Fiorin G, et al. 2014. Structure of water at charged interfaces: a molecular dynamics study. *Langmuir* 30(27):8056–65
41. Finney AR, McPherson IJ, Unwin PR, Salvalaglio M. 2021. Electrochemistry, ion adsorption and dynamics in the double layer: a study of NaCl(aq) on graphite. *Chem. Sci.* 12(33):11166–80
42. Zhu C, Huang K, Siepser NP, Baker LA. 2020. Scanning ion conductance microscopy. *Chem. Rev.* 121(19):11726–68
43. Garcia R. 2020. Nanomechanical mapping of soft materials with the atomic force microscope: methods, theory and applications. *Chem. Soc. Rev.* 49(16):5850–84
44. Ducker WA, Senden TJ, Pashley RM. 1991. Direct measurement of colloidal forces using an atomic force microscope. *Nature* 353(6341):239–41
45. Israelachvili JN. 2011. *Intermolecular and Surface Forces*. Amsterdam: Elsevier. 3rd ed.
46. Derjaguin B, Landau L. 1993. Theory of the stability of strongly charged lyophobic sols and of the adhesion of strongly charged particles in solutions of electrolytes. *Prog. Surf. Sci.* 43(1–4):30–59
47. Butt H-J, Cappella B, Kappl M. 2005. Force measurements with the atomic force microscope: technique, interpretation and applications. *Surf. Sci. Rep.* 59(1–6):1–152
48. Dong Y, Laaksonen A, Cao W, Ji X, Lu X. 2019. AFM study of pH-dependent adhesion of single protein to TiO<sub>2</sub> surface. *Adv. Mater. Interfaces* 6(14):1900411
49. Almonte L, Lopez-Elvira E, Baró AM. 2014. Surface-charge differentiation of streptavidin and avidin by atomic force microscopy-force spectroscopy. *ChemPhysChem* 15(13):2768–73
50. Yang Y, Mayer KM, Hafner JH. 2007. Quantitative membrane electrostatics with the atomic force microscope. *Biophys. J.* 92(6):1966–74
51. Israelachvili JN. 2011. Solvation, structural, and hydration forces. In *Intermolecular and Surface Forces*, ed. JN Israelachvili, pp. 341–80. San Diego, CA: Academic. 3rd ed.
52. Zhmud BV, Meurk A, Bergström L. 2000. Application of charge regulation model for evaluation of surface ionization parameters from atomic force microscopy (AFM) data. *Colloids Surf. A Physicochem. Eng. Asp.* 164(1):3–7
53. Senden TJ, Drummond CJ, Kekicheff P. 1994. Atomic force microscopy: imaging with electrical double layer interactions. *Langmuir* 10(2):358–62
54. Raiteri R, Margesin B, Grattarola M. 1998. An atomic force microscope estimation of the point of zero charge of silicon insulators. *Sens. Actuators B Chem.* 46(2):126–32
55. Zhmud BV, Meurk A, Bergström L. 1998. Evaluation of surface ionization parameters from AFM data. *J. Colloid Interface Sci.* 207(2):332–43
56. Heinz WF, Hoh JH. 1999. Relative surface charge density mapping with the atomic force microscope. *Biophys. J.* 76(1):528–38
57. Zhao C, Ebeling D, Siretanu I, van den Ende D, Mugele F. 2015. Extracting local surface charges and charge regulation behavior from atomic force microscopy measurements at heterogeneous solid-electrolyte interfaces. *Nanoscale* 7(39):16298–311
58. Li L, Steinmetz NF, Eppell SJ, Zypman FR. 2020. Charge calibration standard for atomic force microscope tips in liquids. *Langmuir* 36(45):13621–32
59. Hansma PK, Cleveland JP, Radmacher M, Walters DA, Hillner PE, et al. 1994. Tapping mode atomic force microscopy in liquids. *Appl. Phys. Lett.* 64(13):1738–40
60. Giessibl FJ. 2019. The qPlus sensor, a powerful core for the atomic force microscope. *Rev. Sci. Instrum.* 90(1):011101

61. Giessibl FJ. 2003. Advances in atomic force microscopy. *Rev. Mod. Phys.* 75(3):949–83
62. Fukuma T, Jarvis SP. 2006. Development of liquid-environment frequency modulation atomic force microscope with low noise deflection sensor for cantilevers of various dimensions. *Rev. Sci. Instrum.* 77(4):43701
63. Fukuma T, Kobayashi K, Matsushige K, Yamada H. 2005. True atomic resolution in liquid by frequency-modulation atomic force microscopy. *Appl. Phys. Lett.* 87(3):034101
64. Kobayashi K, Yamada H, Matsushige K. 2009. Frequency noise in frequency modulation atomic force microscopy. *Rev. Sci. Instrum.* 80(4):043708
65. Ueyama H, Sugawara Y, Morita S. 1998. Stable operation mode for dynamic noncontact atomic force microscopy. *Appl. Phys. A Mater. Sci. Process.* 66(7):S295–97
66. Hansma PK, Drake B, Marti O, Gould SAC, Prater CB. 1989. The scanning ion-conductance microscope. *Science* 243(4891):641–43
67. Page A, Perry D, Unwin PR. 2017. Multifunctional scanning ion conductance microscopy. *Proc. R. Soc. A* 473(2200):20160889
68. Chen CC, Zhou Y, Baker LA. 2012. Scanning ion conductance microscopy. *Annu. Rev. Anal. Chem.* 5:207–28
69. Bentley CL, Perry D, Unwin PR. 2018. Stability and placement of Ag/AgCl quasi-reference counter electrodes in confined electrochemical cells. *Anal. Chem.* 90(12):7700–7
70. Momotenko D, McKelvey K, Kang M, Meloni GN, Unwin PR. 2016. Simultaneous interfacial reactivity and topography mapping with scanning ion conductance microscopy. *Anal. Chem.* 88(5):2838–46
71. Teahan J, Perry D, Chen B, McPherson IJ, Meloni GN, Unwin PR. 2021. Scanning ion conductance microscopy: surface charge effects on electroosmotic flow delivery from a nanopipette. *Anal. Chem.* 93(36):12281–88
72. Shi W, Sa N, Thakar R, Baker LA. 2015. Nanopipette delivery: influence of surface charge. *Analyst* 140(14):4835–42
73. Wei C, Bard AJ, Feldberg SW. 1997. Current rectification at quartz nanopipet electrodes. *Anal. Chem.* 69(22):4627–33
74. Siwy ZS. 2006. Ion-current rectification in nanopores and nanotubes with broken symmetry. *Adv. Funct. Mater.* 16(6):735–46
75. White HS, Bund A. 2008. Ion current rectification at nanopores in glass membranes. *Langmuir* 24(5):2212–18
76. Rabinowitz J, Edwards MA, Whittier E, Jayant K, Shepard KL. 2019. Nanoscale fluid vortices and non-linear electroosmotic flow drive ion current rectification in the presence of concentration gradients. *J. Phys. Chem. A* 123(38):8285–93
77. McPherson IJ, Brown P, Meloni GN, Unwin PR. 2021. Visualization of ion fluxes in nanopipettes: detection and analysis of electro-osmosis of the second kind. *Anal. Chem.* 93(49):16302–7
78. Kenis PJA, Ismagilov RF, Takayama S, Whitesides GM, Li S, White HS. 2000. Fabrication inside microchannels using fluid flow. *Acc. Chem. Res.* 33(12):841–47
79. Perry D, Momotenko D, Lazenby RA, Kang M, Unwin PR. 2016. Characterization of nanopipettes. *Anal. Chem.* 88(10):5523–30
80. Sa N, Lan W-J, Shi W, Baker LA. 2013. Rectification of ion current in nanopipettes by external substrates. *ACS Nano* 7(12):11272–82
81. Cremin K, Jones BA, Teahan J, Meloni GN, Perry D, et al. 2020. Scanning ion conductance microscopy reveals differences in the ionic environments of gram-positive and negative bacteria. *Anal. Chem.* 92(24):16024–32
82. Perry D, Page A, Chen B, Frenguelli BG, Unwin PR. 2017. Differential-concentration scanning ion conductance microscopy. *Anal. Chem.* 89(22):12458–65
83. Rheinlaender J, Schäffer TE. 2009. Image formation, resolution, and height measurement in scanning ion conductance microscopy. *J. Appl. Phys.* 105(9):94905
84. Edwards MA, Williams CG, Whitworth AL, Unwin PR. 2009. Scanning ion conductance microscopy: a model for experimentally realistic conditions and image interpretation. *Anal. Chem.* 81(11):4482–92
85. Gramse G, Edwards MA, Fumagalli L, Gomila G. 2012. Dynamic electrostatic force microscopy in liquid media. *Appl. Phys. Lett.* 101(21):213108

86. Hernández-Muñoz J, Chacón E, Tarazona P. 2019. Density functional analysis of atomic force microscopy in a dense fluid. *J. Chem. Phys.* 151(3):034701
87. Kumar N, Andersson MP, van den Ende D, Mugele F, Siretanu I. 2017. Probing the surface charge on the basal planes of kaolinite particles with high-resolution atomic force microscopy. *Langmuir* 33(50):14226–37
88. Butt H-J. 2007. Analyzing electric double layers with the atomic force microscope. In *Encyclopedia of Electrochemistry*, ed. AJ Bard, pp. 236–47. New York: John Wiley & Sons
89. Shevchuk AI, Gorelik J, Harding SE, Lab MJ, Klenerman D, Korchev YE. 2001. Simultaneous measurement of  $\text{Ca}^{2+}$  and cellular dynamics: combined scanning ion conductance and optical microscopy to study contracting cardiac myocytes. *Biophys. J.* 81(3):1759–64
90. Hillier AC, Kim S, Bard AJ. 1996. Measurement of double-layer forces at the electrode/electrolyte interface using the atomic force microscope: potential and anion dependent interactions. *J. Phys. Chem.* 100(48):18808–17
91. Hu K, Fan F-RF, Bard AJ, Hillier AC. 1997. Direct measurement of diffuse double-layer forces at the semiconductor/electrolyte interface using an atomic force microscope. *J. Phys. Chem. B* 101(41):8298–303
92. Butt H-J, Jaschke M, Ducker W. 1995. Measuring surface forces in aqueous electrolyte solution with the atomic force microscope. *Bioelectrochem. Bioenerg.* 38(1):191–201
93. Miyatani T, Horii M, Rosa A, Fujihira M, Marti O. 1997. Mapping of electrical double-layer force between tip and sample surfaces in water with pulsed-force-mode atomic force microscopy. *Appl. Phys. Lett.* 71(18):2632–34
94. Kobayashi N, Asakawa H, Fukuma T. 2010. Nanoscale potential measurements in liquid by frequency modulation atomic force microscopy. *Rev. Sci. Instrum.* 81(12):123705
95. Hu K, Chai Z, Whitesell JK, Bard AJ. 1999. In situ monitoring of diffuse double layer structure changes of electrochemically addressable self-assembled monolayers with an atomic force microscope. *Langmuir* 15(9):3343–47
96. Wang J, Bard AJ. 2001. Direct atomic force microscopic determination of surface charge at the gold/electrolyte interface—the inadequacy of classical GCS theory in describing the double-layer charge distribution. *J. Phys. Chem. B* 105(22):5217–22
97. Wang J, Bard AJ. 2001. On the absence of a diffuse double layer at electronically conductive polymer film electrodes. Direct evidence by atomic force microscopy of complete charge compensation. *J. Am. Chem. Soc.* 123(3):498–99
98. Wang J, Feldberg SW, Bard AJ. 2002. Measurement of double-layer forces at the polymer film/electrolyte interfaces using atomic force microscopy: concentration and potential-dependent interactions. *J. Phys. Chem. B* 106(40):10440–46
99. Hernando-Pérez M, Cartagena-Rivera AX, Božič AL, Carrillo PJP, San Martín C, et al. 2015. Quantitative nanoscale electrostatics of viruses. *Nanoscale* 7(41):17289–98
100. Sotres J, Baró AM. 2010. AFM imaging and analysis of electrostatic double layer forces on single DNA molecules. *Biophys. J.* 98(9):1995–2004
101. Rosa-Zeiser A, Weilandt E, Hild S, Marti O. 1997. The simultaneous measurement of elastic, electrostatic and adhesive properties by scanning force microscopy: pulsed-force mode operation. *Meas. Sci. Technol.* 8(11):1333–38
102. Miyatani T, Okamoto S, Rosa A, Marti O, Fujihira M. 1998. Surface charge mapping of solid surfaces in water by pulsed-force-mode atomic force microscopy. *Appl. Phys. A Mater. Sci. Process.* 66(7):S349–52
103. Kobayashi N, Asakawa H, Fukuma T. 2011. Quantitative potential measurements of nanoparticles with different surface charges in liquid by open-loop electric potential microscopy. *J. Appl. Phys.* 110(4):044315
104. Gramse G, Dols-Perez A, Edwards MA, Fumagalli L, Gomila G. 2013. Nanoscale measurement of the dielectric constant of supported lipid bilayers in aqueous solutions with electrostatic force microscopy. *Biophys. J.* 104(6):1257–62

105. Su S, Siretanu I, Ende D, Mei B, Mul G, Mugele F. 2021. Facet-dependent surface charge and hydration of semiconducting nanoparticles at variable pH. *Adv. Mater.* 33(52):2106229
106. Umeda K, Kobayashi K, Oyabu N, Matsushige K, Yamada H. 2015. Molecular-scale quantitative charge density measurement of biological molecule by frequency modulation atomic force microscopy in aqueous solutions. *Nanotechnology* 26(28):285103
107. Martínez NF, Lozano JR, Herruzo ET, Garcia F, Richter C, et al. 2008. Bimodal atomic force microscopy imaging of isolated antibodies in air and liquids. *Nanotechnology* 19(38):384011
108. Sa N, Baker LA. 2011. Rectification of nanopores at surfaces. *J. Am. Chem. Soc.* 133(27):10398–401
109. Ma Y, Liu R, Shen X, Wang D. 2021. Quantification of asymmetric ion transport in glass nanopipettes near charged substrates. *ChemElectroChem* 8(20):3917–22
110. Zhou Y, Chen C-C, Weber AE, Zhou L, Baker LA, Hou J. 2013. Potentiometric-scanning ion conductance microscopy for measurement at tight junctions. *Tissue Barriers* 1(4):e25585
111. Chen C-C, Baker LA. 2011. Effects of pipette modulation and imaging distances on ion currents measured with Scanning Ion Conductance Microscopy (SICM). *Analyst* 136(1):90–97
112. McKelvey K, Perry D, Byers JC, Colburn AW, Unwin PR. 2014. Bias modulated scanning ion conductance microscopy. *Anal. Chem.* 86(7):3639–46
113. Klausen LH, Fuhs T, Dong M. 2016. Mapping surface charge density of lipid bilayers by quantitative surface conductivity microscopy. *Nat. Commun.* 7(1):12447
114. Edmondson JF, Meloni GN, Costantini G, Unwin PR. 2020. Synchronous electrical conductance- and electron tunnelling-scanning electrochemical microscopy measurements. *ChemElectroChem* 7(3):697–706
115. Fuhs T, Klausen LH, Sønderkov SM, Han X, Dong M. 2018. Direct measurement of surface charge distribution in phase separating supported lipid bilayers. *Nanoscale* 10(9):4538–44
116. Sønderkov SM, Klausen LH, Skaanvik SA, Han X, Dong M. 2020. In situ surface charge density visualization of self-assembled DNA nanostructures after ion exchange. *ChemPhysChem* 21(13):1474–82
117. Wang D, Brown W, Li Y, Kvetny M, Liu J, Wang G. 2017. Correlation of ion transport hysteresis with the nanogeometry and surface factors in single conical nanopores. *Anal. Chem.* 89(21):11811–17
118. Ma Y, Wang D. 2021. Revealing electrical double-layer potential of substrates by hysteresis ion transport in scanning ion conductance microscopy. *Anal. Chem.* 93(48):15821–25
119. Chen F, He J, Manandhar P, Yang Y, Liu P, Gu N. 2021. Gauging surface charge distribution of live cell membrane by ionic current change using scanning ion conductance microscopy. *Nanoscale* 13(47):19973–84
120. Chen F, Manandhar P, Ahmed MS, Chang S, Panday N, et al. 2019. Extracellular surface potential mapping by scanning ion conductance microscopy revealed transient transmembrane pore formation induced by conjugated polymer nanoparticles. *Macromol. Biosci.* 19(2):e1800271
121. Chen F, Panday N, Li X, Ma T, Guo J, et al. 2020. Simultaneous mapping of nanoscale topography and surface potential of charged surfaces by scanning ion conductance microscopy. *Nanoscale* 12(40):20737–48
122. Zhou Y, Chen C-C, Weber AE, Zhou L, Baker LA. 2014. Potentiometric-scanning ion conductance microscopy. *Langmuir* 30(19):5669–75
123. Chen C-C, Zhou Y, Morris CA, Hou J, Baker LA. 2013. Scanning ion conductance microscopy measurement of paracellular channel conductance in tight junctions. *Anal. Chem.* 85(7):3621–28
124. Attwood SJ, Kershaw R, Uddin S, Bishop SM, Welland ME. 2019. Understanding how charge and hydrophobicity influence globular protein adsorption to alkanethiol and material surfaces. *J. Mater. Chem. B* 7(14):2349–61
125. Tao L, Qiao M, Jin R, Li Y, Xiao Z, et al. 2019. Bridging the surface charge and catalytic activity of a defective carbon electrocatalyst. *Angew. Chem. Int. Ed.* 58(4):1019–24
126. Payne NA, Dawkins JIG, Schougaard SB, Mauzeroll J. 2019. Effect of substrate permeability on scanning ion conductance microscopy: uncertainty in tip-substrate separation and determination of ionic conductivity. *Anal. Chem.* 91(24):15718–25
127. Kumar N, Zhao C, Klaassen A, van den Ende D, Mugele F, Siretanu I. 2016. Characterization of the surface charge distribution on kaolinite particles using high resolution atomic force microscopy. *Geochim. Cosmochim. Acta* 175:100–12

128. Siretanu I, Ebeling D, Andersson MP, Stipp SLS, Philipse A, et al. 2014. Direct observation of ionic structure at solid-liquid interfaces: a deep look into the Stern layer. *Sci. Rep.* 4(1):4956
129. Chen C, Petterson T, Illergård J, Ek M, Wågberg L. 2019. Influence of cellulose charge on bacteria adhesion and viability to PVAm/CNF/PVAm-modified cellulose model surfaces. *Biomacromolecules* 20(5):2075–83
130. Ushiki T, Ishizaki K, Mizutani Y, Nakajima M, Iwata F. 2021. Scanning ion conductance microscopy of isolated metaphase chromosomes in a liquid environment. *Chromosome Res.* 29(1):95–106
131. Chen B, Perry D, Page A, Kang M, Unwin PR. 2019. Scanning ion conductance microscopy: quantitative nanopipette delivery-substrate electrode collection measurements and mapping. *Anal. Chem.* 91(3):2516–24
132. Strelcov E, Arble C, Guo H, Hoskins BD, Yulaev A, et al. 2020. Nanoscale mapping of the double layer potential at the graphene-electrolyte interface. *Nano Lett.* 20(2):1336–44
133. Jin R, Huang Y, Cheng L, Lu H, Jiang D, Chen H-Y. 2020. In situ observation of heterogeneous charge distribution at the electrode unraveling the mechanism of electric field-enhanced electrochemical activity. *Chem. Sci.* 11(16):4158–63
134. Chen C-H, Luo S-C. 2015. Tuning surface charge and morphology for the efficient detection of dopamine under the interferences of uric acid, ascorbic acid, and protein adsorption. *ACS Appl. Mater. Interfaces* 7(39):21931–38
135. Yang C-W, Miyazawa K, Fukuma T, Miyata K, Hwang I-S. 2018. Direct comparison between subnanometer hydration structures on hydrophilic and hydrophobic surfaces via three-dimensional scanning force microscopy. *Phys. Chem. Chem. Phys.* 20(36):23522–27
136. Hirata K, Kitagawa T, Miyazawa K, Okamoto T, Fukunaga A, et al. 2018. Visualizing charges accumulated in an electric double layer by three-dimensional open-loop electric potential microscopy. *Nanoscale* 10(30):14736–46
137. Patel AN, Collignon MG, O'Connell MA, Hung WOY, McKelvey K, et al. 2012. A new view of electrochemistry at highly oriented pyrolytic graphite. *J. Am. Chem. Soc.* 134(49):20117–30
138. Lai SCS, Patel AN, McKelvey K, Unwin PR. 2012. Definitive evidence for fast electron transfer at pristine basal plane graphite from high-resolution electrochemical imaging. *Angew. Chem. Int. Ed.* 51(22):5405–8
139. Unwin PR, Güell AG, Zhang G. 2016. Nanoscale electrochemistry of sp<sup>2</sup> carbon materials: from graphite and graphene to carbon nanotubes. *Acc. Chem. Res.* 49(9):2041–48
140. Shi W, Sa N, Thakar R, Baker LA. 2015. Nanopipette delivery: influence of surface charge. *Analyst* 140(14):4835–42
141. Chen B, Perry D, Teahan J, McPherson JJ, Edmondson J, et al. 2021. Artificial synapse: spatiotemporal heterogeneities in dopamine electrochemistry at a carbon fiber ultramicroelectrode. *ACS Meas. Sci. Au* 1(1):6–10
142. Gan Y, Franks GV. 2006. Charging behavior of the gibbsite basal (001) surface in NaCl solution investigated by AFM colloidal probe technique. *Langmuir* 22(14):6087–92
143. Herruzo ET, Asakawa H, Fukuma T, Garcia R. 2013. Three-dimensional quantitative force maps in liquid with 10 piconewton, angstrom and sub-minute resolutions. *Nanoscale* 5(7):2678–85
144. Uhlig MR, Benaglia S, Thakkar R, Comer J, Garcia R. 2021. Atomically resolved interfacial water structures on crystalline hydrophilic and hydrophobic surfaces. *Nanoscale* 13(10):5275–83
145. Zhu C, Jagdale G, Gandolfo A, Alanis K, Abney R, et al. 2021. Surface charge measurements with scanning ion conductance microscopy provide insights into nitrous acid speciation at the kaolin mineral-air interface. *Environ. Sci. Technol.* 55(18):12233–42
146. Kominami H, Kobayashi K, Yamada H. 2019. Molecular-scale visualization and surface charge density measurement of Z-DNA in aqueous solution. *Sci. Rep.* 9(1):6851
147. Yamamoto Y, Kominami H, Kobayashi K, Yamada H. 2021. Surface charge density measurement of a single protein molecule with a controlled orientation by AFM. *Biophys. J.* 120(12):2490–97
148. Ushiki T, Ishizaki K, Mizutani Y, Nakajima M, Iwata F. 2021. Scanning ion conductance microscopy of isolated metaphase chromosomes in a liquid environment. *Chromosome Res.* 29(1):95–106
149. Novak P, Li C, Shevchuk AI, Stepanyan R, Caldwell M, et al. 2009. Nanoscale live-cell imaging using hopping probe ion conductance microscopy. *Nat. Methods* 6(4):279–81

150. Sader JE, Chon JWM, Mulvaney P. 1999. Calibration of rectangular atomic force microscope cantilevers. *Rev. Sci. Instrum.* 70(10):3967–69
151. Sun L, Shigyou K, Ando T, Watanabe S. 2019. Thermally driven approach to fill sub-10-nm pipettes with batch production. *Anal. Chem.* 91(21):14080–84
152. Takahashi Y, Zhou Y, Miyamoto T, Higashi H, Nakamichi N, et al. 2020. High-speed SICM for the visualization of nanoscale dynamic structural changes in hippocampal neurons. *Anal. Chem.* 92(2):2159–67